

XEROCOPY RESOLUTION TEST CHART

12

AD-A175 151

Electron Cyclotron Harmonic Waves Observed by the AMPTE-IRM Plasma Wave Experiment Following a Lithium Release in the Solar Wind

J. L. ROEDER and H. C. KOONS
Space Sciences Laboratory
Laboratory Operations
The Aerospace Corporation
El Segundo, CA 90245

R. H. HOLZWORTH
University of Washington
Space Sciences Division
Seattle, WA 98195

R. R. ANDERSON and D. A. GURNETT
University of Iowa
Department of Physics and Astronomy
Iowa City, IA 52242

and

O. H. BAUER, G. HAERENDEL, B. HAEUSLER, and R. TREUMANN
Max Planck Institute for Physics and Astrophysics
Institute for Extraterrestrial Physics
Federal Republic of Germany

1 November 1986

APPROVED FOR PUBLIC RELEASE;
DISTRIBUTION UNLIMITED

DTIC
ELECTE
DEC 18 1986
S
D

DTIC FILE COPY

Prepared for
SPACE DIVISION
AIR FORCE SYSTEMS COMMAND
Los Angeles Air Force Station
P.O. Box 92960, Worldway Postal Center
Los Angeles, CA 90009-2960

This report was submitted by The Aerospace Corporation, El Segundo, CA 90245, under Contract No. F04701-85-C-0086-P00016 with the Space Division, P.O. Box 92960, Worldway Postal Center, Los Angeles, CA 90009-2960. It was reviewed and approved for The Aerospace Corporation by H. R. Rugge, Director, Space Sciences Laboratory.

Capt Douglas R. Case/YCM was the project officer for the Mission-Oriented Investigation and Experimentation (MOIE) Program.

This report has been reviewed by the Public Affairs Office (PAS) and is releasable to the National Technical Information Service (NTIS). At NTIS, it will be available to the general public, including foreign nationals.

This technical report has been reviewed and is approved for publication. Publication of this report does not constitute Air Force approval of the report's findings or conclusions. It is published only for the exchange and stimulation of ideas.



DOUGLAS R. CASE, Capt, USAF
MOIE Project Officer
SD/YCM



JOSEPH HESS, GM-15
Director, AFSTC West Coast Office
AFSTC/WCO OL-AB

UNCLASSIFIED

SECURITY CLASSIFICATION OF THIS PAGE (When Data Entered)

REPORT DOCUMENTATION PAGE		READ INSTRUCTIONS BEFORE COMPLETING FORM
1. REPORT NUMBER SD-TR-86-71	2. GOVT ACCESSION NO.	3. RECIPIENT'S CATALOG NUMBER
4. TITLE (and Subtitle) ELECTRON CYCLOTRON HARMONIC WAVES OBSERVED BY THE AMPTE-IRM PLASMA WAVE EXPERIMENT FOLLOWING A LITHIUM RELEASE IN THE SOLAR WIND		5. TYPE OF REPORT & PERIOD COVERED
		6. PERFORMING ORG. REPORT NUMBER TR-0086(6940-06)-4
7. AUTHOR(s) James L. Roeder, Harry C. Koons, R. H. Holzworth, R. R. Anderson, D. A. Gurnett, O. H. Bauer, G. Haerendel, B. Haeusler, and R. Treumann		8. CONTRACT OR GRANT NUMBER(s) F04701-85-C-0086-P00016
9. PERFORMING ORGANIZATION NAME AND ADDRESS The Aerospace Corporation El Segundo, CA 90245		10. PROGRAM ELEMENT, PROJECT, TASK AREA & WORK UNIT NUMBERS
11. CONTROLLING OFFICE NAME AND ADDRESS Space Division Los Angeles Air Force Station Los Angeles, CA 90009-2960		12. REPORT DATE 1 November 1986
		13. NUMBER OF PAGES 30
14. MONITORING AGENCY NAME & ADDRESS (if different from Controlling Office)		15. SECURITY CLASS. (of this report) Unclassified
		15a. DECLASSIFICATION/DOWNGRADING SCHEDULE
16. DISTRIBUTION STATEMENT (of this Report) Approved for public release; distribution unlimited.		
17. DISTRIBUTION STATEMENT (of the abstract entered in Block 20, if different from Report)		
18. SUPPLEMENTARY NOTES		
19. KEY WORDS (Continue on reverse side if necessary and identify by block number) plasma waves, chemical release, solar wind		
20. ABSTRACT (Continue on reverse side if necessary and identify by block number) An unexpected occurrence following the second lithium release by the AMPTE-IRM spacecraft in the solar wind on September 20, 1984 was the appearance of electrostatic electron harmonic (ECH) emissions. These emissions began about 50 sec after the release and continued for several minutes. Narrow band emissions polarized perpendicular to the magnetic field were present in each of the first five harmonic bands. Unpolarized broadband emissions were also present at the same time. The broadband emissions extended from below the electron cyclotron frequency to above the highest ECH band. Both		

DD FORM 1473
(FACSIMILE)UNCLASSIFIED
SECURITY CLASSIFICATION OF THIS PAGE (When Data Entered)

UNCLASSIFIED

SECURITY CLASSIFICATION OF THIS PAGE(When Data Entered)

19. KEY WORDS (Continued)

20. ABSTRACT (Continued)

emissions were entirely electrostatic because no accompanying signals were detected by the magnetic antenna. Candidate generation processes include the ion acoustic and the electron cyclotron drift instabilities. These instabilities would be driven by the relative drift of the lithium ions and the solar wind electrons. It will be shown that the calculated growth rates of these processes are sufficient to account for the measured waves, but that the observed lack of a Doppler shift of the ECH bands is inconsistent with the theory. *Chen, S. H.*

UNCLASSIFIED

SECURITY CLASSIFICATION OF THIS PAGE(When Data Entered)

PREFACE

We wish to express our appreciation to our many colleagues who participated in the development, testing, integration, and data reduction for this experiment. In particular, we acknowledge the efforts of K. Gnaiger (KGM), F. Eberl (MPE), D. Odem and R. D. Anderson (University of Iowa), W. B. Harbridge, A. Allard, D. Katsuda, and D. Bax (The Aerospace Corporation).

Accession For	
NTIS CRA&I	<input checked="" type="checkbox"/>
DTIC TAB	<input type="checkbox"/>
Unannounced	<input type="checkbox"/>
Justification	
By	
Distribution/	
Availability Codes	
Dist	Avail and/or Special
A-1	



CONTENTS

PREFACE.....	1
INTRODUCTION.....	9
INSTRUMENTATION.....	11
OBSERVATIONS.....	11
MODEL RESULTS.....	25
CONCLUSION.....	31
REFERENCES.....	33

FIGURES

1.	Spectrogram of 15 min of Electric and Magnetic Field Amplitudes over the Frequency Range 200 Hz-100 kHz.....	13
2.	Average Spectrums of the Electric Emissions Observed Within Each of Four Bins of the Angle Between the Dipole Antenna and the Projection of the Magnetic Field on the Spin Plane of the Spacecraft.....	15
3.	Spectrograms of 30 sec of Electric Field Amplitudes from the Two Wideband Receivers and the Antenna Spin Phase Angle.....	17
4.	A Composite Spectrum of the Electric Field Amplitude During the Interval 0957:50 - 0957:52 UT.....	19
5.	The Measured Number Density and Drift Energy of the Lithium Ions During the ECH Emissions.....	21
6.	Schematic Diagram of the Vector Geometry Needed to Compute the Relative Velocity of the Lithium Ions and the Solar Wind Electrons.....	27
7.	Model Frequencies and Temporal Growth Rates for the First Four Harmonics Due To the Electron Cyclotron Drift Instability.....	29

TABLE

1. Plasma Parameters During the ECH Emissions..... 23

INTRODUCTION

The Active Magnetospheric Particle Tracer Explorers (AMPTE) program performed two lithium releases in the solar wind upstream of the earth's bow shock in September, 1984. An unpredicted occurrence following the second lithium release was the appearance of electrostatic emissions near the harmonics of the electron cyclotron frequency. Similar harmonic waves were not observed during the first AMPTE lithium release. The analysis and interpretation of these waves are presented in this report.

The AMPTE program is a series of active experiments with two purposes: to study the access of solar wind ions to the magnetosphere, and to investigate the physics of the interaction of an injected plasma cloud with an existing cosmical plasma [Krimigis et al., 1982; Bryant et al., 1985]. Three spacecraft are involved in the AMPTE project: the Ion Release Module (IRM) which releases the chemical canisters, the United Kingdom Subsatellite (UKS) which orbits near the IRM to study the expansion and evolution of the releases, and the Charge Composition Explorer (CCE) which searches for the tracer ions in the inner regions of the magnetosphere. The data presented in this report were obtained from the plasma diagnostic instruments aboard the IRM. The orbit of the IRM is highly elliptical with a period of 44 h, a 28.5° inclination, and an apogee of 19.5 earth radii. During the September, 1984 releases the IRM was at apogee on the dayside of the earth near local noon.

INSTRUMENTATION

The electric field emissions described in this report were measured by the IRM plasma wave instrument described in detail by Haeusler et al. [1985]. This instrument uses a 47 m tip-to-tip electric dipole antenna for electric field measurements and two search coil antennas for low frequency and high frequency magnetic field measurements. The signals from the antennas were processed by a variety of onboard spectrum analyzers covering the frequency range 31 Hz - 5.6 MHz. These include a Stepped Frequency Receiver (SFR), which is a fully synthesized 96-channel analyzer from 200 Hz to 100 kHz. The AC electric field was also telemetered to the ground via two wide-band analog channels with bandwidths from 650 Hz to 10 kHz, and from 5 Hz to 1 kHz, respectively. The sensitivity of the electric field measurement is set by the system noise level which is approximately $2 \times 10^{-7} \text{ V m}^{-1} \text{ Hz}^{-1/2}$ in the frequency range 100-1000 Hz.

OBSERVATIONS

The lithium was released into the solar wind for the second time at 0956:02 UT on September 20, 1984. The interplanetary magnetic field before and well after the release was of magnitude 9 nT inclined at an angle of 66° to the solar wind velocity vector of magnitude 460 km/s. A summary of the physical properties of the release is given by Haerendel et al. [1985]. The release generated a diamagnetic cavity around the IRM spacecraft for approximately 7 s as described by Luhr et al. [1985]. After the cavity was convected downstream the solar wind was still strongly disturbed for approximately 1 minute. Because of the long ionization time constant of lithium (~1 hr) the solar wind after

this time was almost undisturbed due to the release. The electron cyclotron harmonic waves were observed in the interval 1-4 minutes after the injection. During the time period when these waves were observed the magnitude of the measured magnetic field remained at 8.9 ± 0.3 nT. This value is within ten percent of its pre-release condition.

A spectrogram of 15 minutes of data from the SFR is shown in Figure 1. The spectrogram is partitioned into three panels, each of which displays the data from a 32 channel analyzer producing one spectrum per second. The bottom panel shows the magnetic data in the frequency range 0.2-2.5 kHz, the middle panel shows the electric data in a similar frequency range, and the top panel shows the electric data from 9 kHz to 99 kHz. The linear frequency scales are marked on the left side of the figure. The data are color-coded according to the scale on the right side of the figure. The horizontal red lines at the bottom of each panel are calibration signals and represent approximately the largest amplitude allowable for each analyzer. The abscissa is marked with the Universal time, the spacecraft geocentric distance in earth radii, and the local time in hours.

The spiked feature in the middle panel is a ten second interval of very intense electric noise which began seven seconds after the injection. This emission has been interpreted as the result of a ion beam-plasma instability within an electrostatic shock at the upstream edge of the lithium cloud [Gurnett et al., 1985]. From 17 seconds to 50 seconds after injection there was a period of relative quiet. Then there began a broadband emission from less than 5 Hz to several kilohertz. Superimposed on the spectrum of the broadband waves were

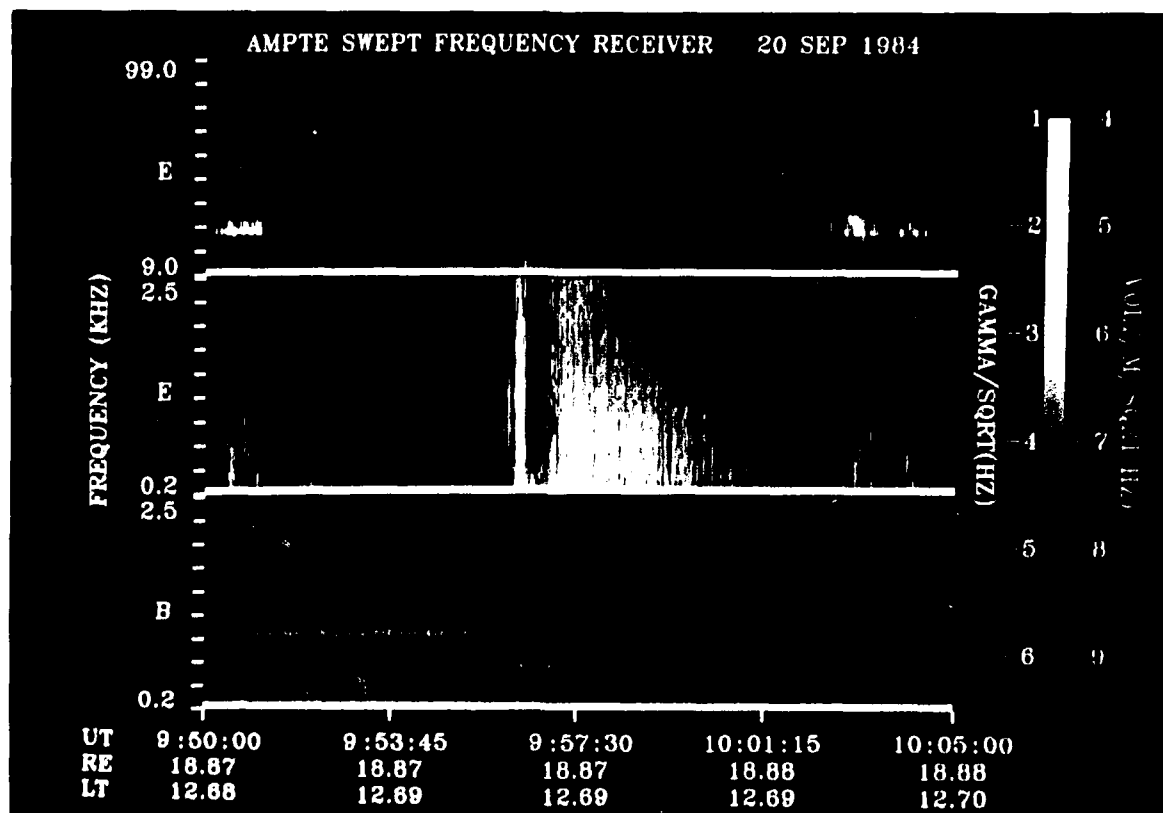


Figure 1. Spectrogram of 15 min of Electric and Magnetic Field Amplitudes over the Frequency Range 200 Hz-100 kHz. The lithium release occurred at 0956:02 UT.

enhancements at frequency intervals of the electron cyclotron frequency. These electron cyclotron harmonic (ECH) emissions and broadband emissions continued for several minutes, with a decreasing upper cutoff frequency, as shown by Figure 1. They are identified by the faint horizontal banding in the middle panel of the spectrogram. The absence of any accompanying magnetic signal in the bottom panel for the emissions observed on the electric antenna means that all of the waves observed were entirely electrostatic. The horizontal lines in the magnetic spectrogram are spacecraft interference.

The line emission in the top panel of Figure 1 at a frequency of 25 kHz is interpreted as an emission at the local electron plasma frequency [Anderson et al., 1985]. This frequency corresponds to an electron density of 8 cm^{-3} . The lines at 50 kHz and 75 kHz correspond to the second and third harmonic of the electron plasma frequency. The plasma frequency emission intensifies during the interval 1002-1004 UT. Since this phenomenon also occurs before 0956 UT, it is probably not related to the release experiment. Similar intensifications and the existence of the emissions at the harmonics of the plasma frequency are interpreted as evidence of a nonlinear mode conversion process by Koons et al. [1985].

Figure 2 shows a measurement of the polarization of the emissions with respect to the magnetic field. The SFR data was sorted and averaged into four bins on the basis of the angle between the electric dipole antenna and the measured magnetic field. The boundaries of each angular bin are shown at the bottom of the figure. The angle between the magnetic field and the spacecraft spin vector is $20\text{-}30^\circ$ so that

AMPTE-IRM Swept Frequency Receiver

SEPTEMBER 20, 1984

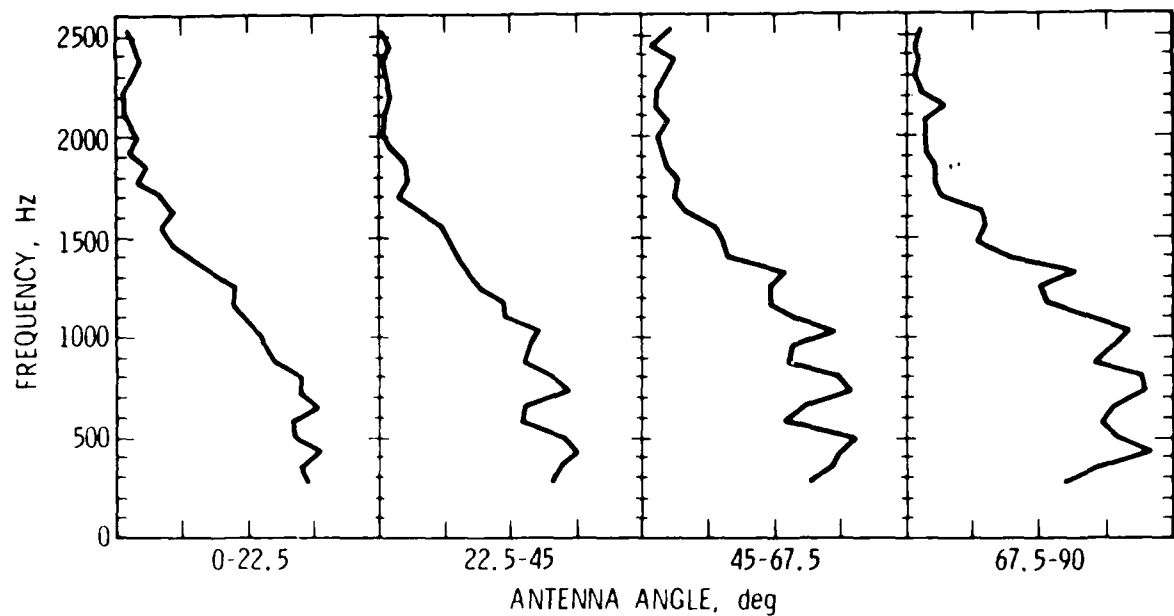


Figure 2. Average Spectrums of the Electric Emissions Observed Within Each of Four Bins of the Angle Between the Dipole Antenna and the Projection of the Magnetic Field on the Spin Plane of the Spacecraft

electric field components are measured at angles in the range 60-90° to the magnetic field. This analysis illustrates that the ECH emissions tend to be polarized in the direction perpendicular to the magnetic field while the broadband waves seem isotropic. There is some amount of mixing of data between adjacent bins because of the short spin period of 4.5 s compared to the 1 s sweep time of the SFR. This means that during the processing of a single spectrum the antenna will rotate through almost 180°, smearing some of the angular dependence of the waves.

Figure 3 shows thirty seconds of data from the wideband receiver aboard the IRM. The electric field waveform information is transmitted to the ground in two AGC-controlled wideband channels: one covering the frequency range 650 Hz to 10 kHz, and a second channel for the frequency range 5 Hz to 1 kHz. The top panel of the figure is a spectrogram of the high frequency channel in the range 0-2 kHz. The middle panel is a spectrogram of the low frequency data over the range 0-1 kHz. The harmonic line structure of the emissions is clearly evident in the spectrograms. The bottom panel displays as a function of time the angle between the antenna and the magnetic field. As the antenna becomes perpendicular to the magnetic field the harmonic emissions increase in amplitude. The automatic gain control of the receivers causes the broadband emission to disappear from the spectrogram at these times in the spin period. This effect is very pronounced at several times in the figure, for example at 0958:10.5 UT and again at 0958:21.5 UT. The absolute amplitude of the broadband emission is nearly isotropic, as shown by SFR data in Figure 2. The electron cyclotron frequency during this interval was constant at 250 Hz, so that the emission lines in the top spectrogram are within the third, fourth, and fifth harmonic bands.

AMPTE-IRM ELECTRIC FIELD
SEPTEMBER 20, 1984

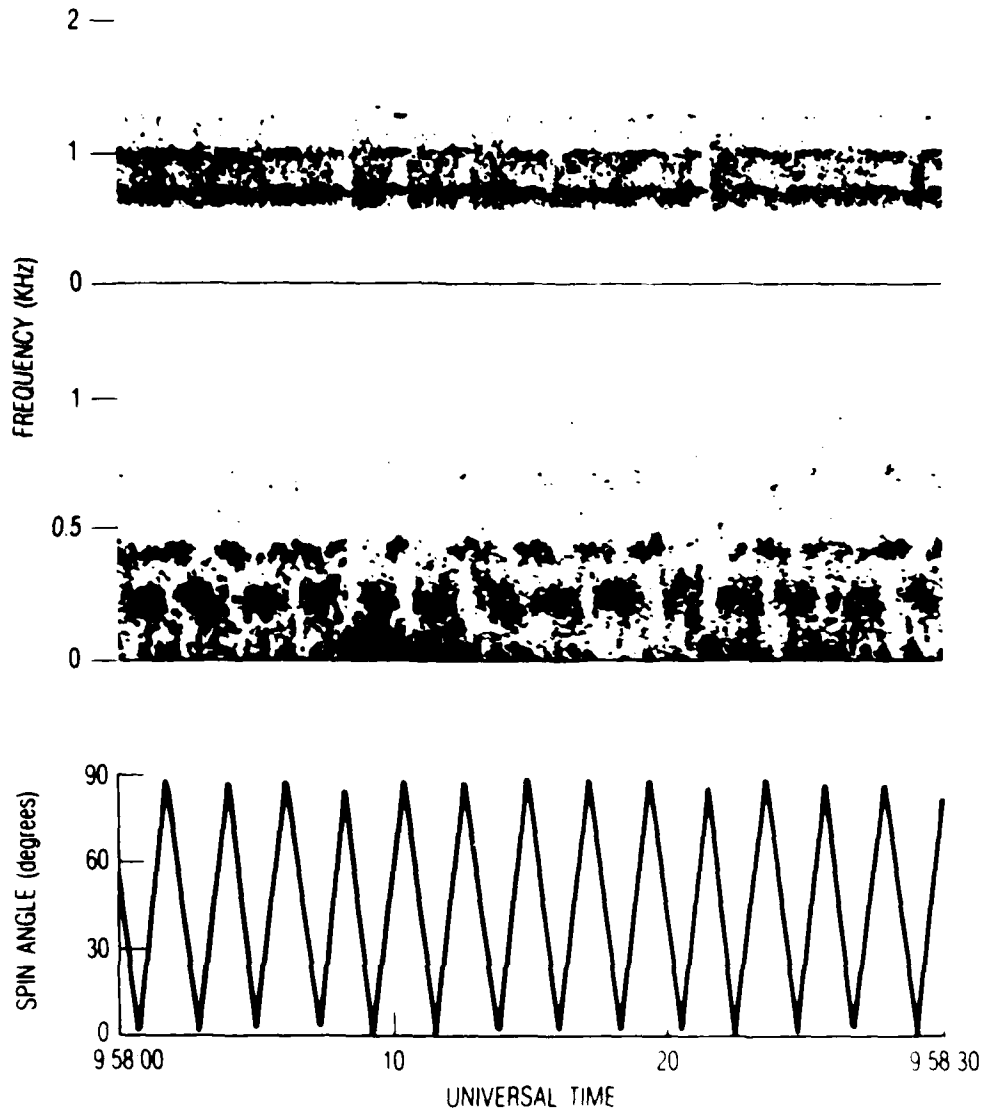


Figure 3. Spectrograms of 30 sec of Electric Field Amplitudes from the Two Wideband Receivers and the Antenna Spin Phase Angle

The emissions visible in the low frequency spectrogram are centered at 450 Hz and 250 Hz.

Figure 4 is a composite spectrum of the wideband data during the period 0957:50 - 0957:52 UT. The antenna was approximately perpendicular to the magnetic field during this interval. The data from the low frequency receiver is plotted as a solid line and the high frequency data is displayed as a dashed line. The amplitude scales of the two receivers have not been intercalibrated. The frequencies of the local electron cyclotron frequency and the first five harmonics are marked by arrows. Narrowband emissions were observed at 435 Hz, 732 Hz, 1014 Hz, 1292 Hz, and 1566 Hz. These frequencies are 1.8, 3.0, 4.2, 5.3, and 6.4 when normalized to the local electron cyclotron frequency. The bandwidths of the emissions were very small ($\Delta f/f \sim 0.05$). The frequencies and bandwidths of the ECH emissions remained approximately constant throughout the entire period in which they were observed.

The observations of the local plasma population were performed by the IRM [Paschmann et al., 1985] and the UKS [Hall et al., 1985]. These data have shown that during the observations of the ECH waves the electron distribution was essentially identical with the pre-release solar wind. The solar wind electron velocity distribution is well represented by a two part isotropic distribution drifting at the solar wind velocity of 460 km/s. The major component had a temperature of 18 eV and a density of 8 cm^{-3} . A tenuous higher energy tail was provided by a second component of temperature of 26 eV and density of 0.2 cm^{-3} . The total electron density computed from the particle data is 8.2 cm^{-3} . This value is in close agreement with the density of 8 cm^{-3} obtained

AMPTE-IRM Electric Field
957:50 UT, September 20, 1984

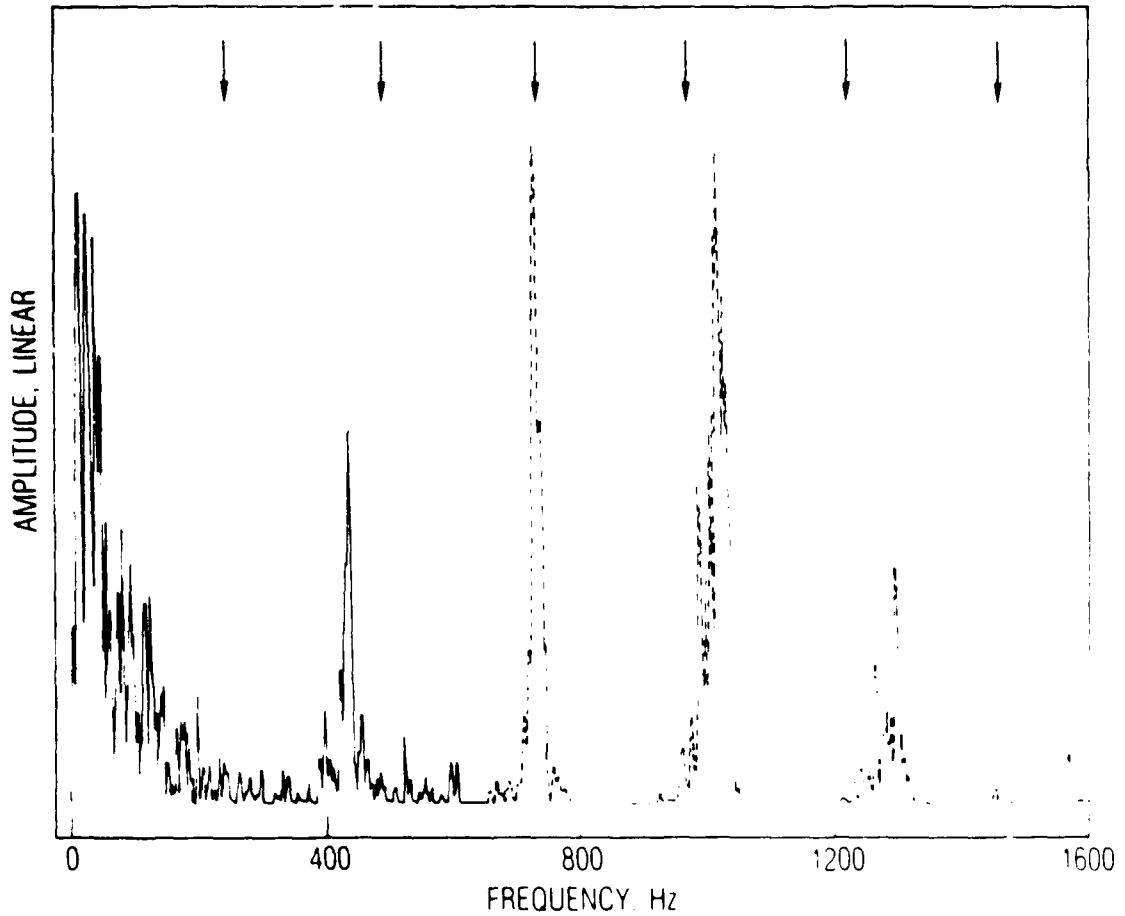


Figure 4. A Composite Spectrum of the Electric Field Amplitude During the Interval 0957:50 - 0957:52 UT. The solid line represents data from the high frequency channel, and low frequency data is shown as a dashed line. The frequencies of the local electron cyclotron frequency are marked by arrows at the top of the panel.

from the plasma wave data [Anderson et al., 1985]. The good agreement of the two electron density measurements indicates that any additional component of the electrons of energy below 15 eV is very small. This discussion neglects the small number of electrons produced by the lithium ionization reaction. It is assumed that these electrons were continually swept up by the solar wind within a cyclotron period so that the entire electron distribution is drifting at the solar wind velocity.

The lithium ions generated by the release were observed by two experiments on the IRM: the plasma instrument [Paschmann et al., 1985] and the time-of-flight ion spectrometer SULEICA [Mobius et al., 1985]. The release cloud is assumed to take the form of an expanding spherical shell of neutral atoms ionized by sunlight, producing ions at rest with a temperature estimated to be approximately 0.2 eV [Haerendel et al., 1985]. These ions are then accelerated perpendicular to the interplanetary magnetic field by the solar wind electric field. Since the density of ions is by this time too low to affect the natural fields and plasma, the ions should behave as test particles. Assuming that the inhomogeneities in the fields are small over an lithium cyclotron radius (approximately 1000 km for a 1 keV ion), the lithium ions should have traced a cycloidal path perpendicular to the magnetic field [Mobius et al., 1985]. But the time interval between the ionization of the lithium and the observation of the ECH waves is short compared with the lithium cyclotron period which is 51 s. This means that all the ions traveled only a small portion of the cycloid phase and that the lithium velocity distribution was that of a beam in the direction perpendicular to the magnetic field. This concept of the lithium ions is essentially confirmed by the observations [Paschmann et al., 1985]. Figure 5 shows

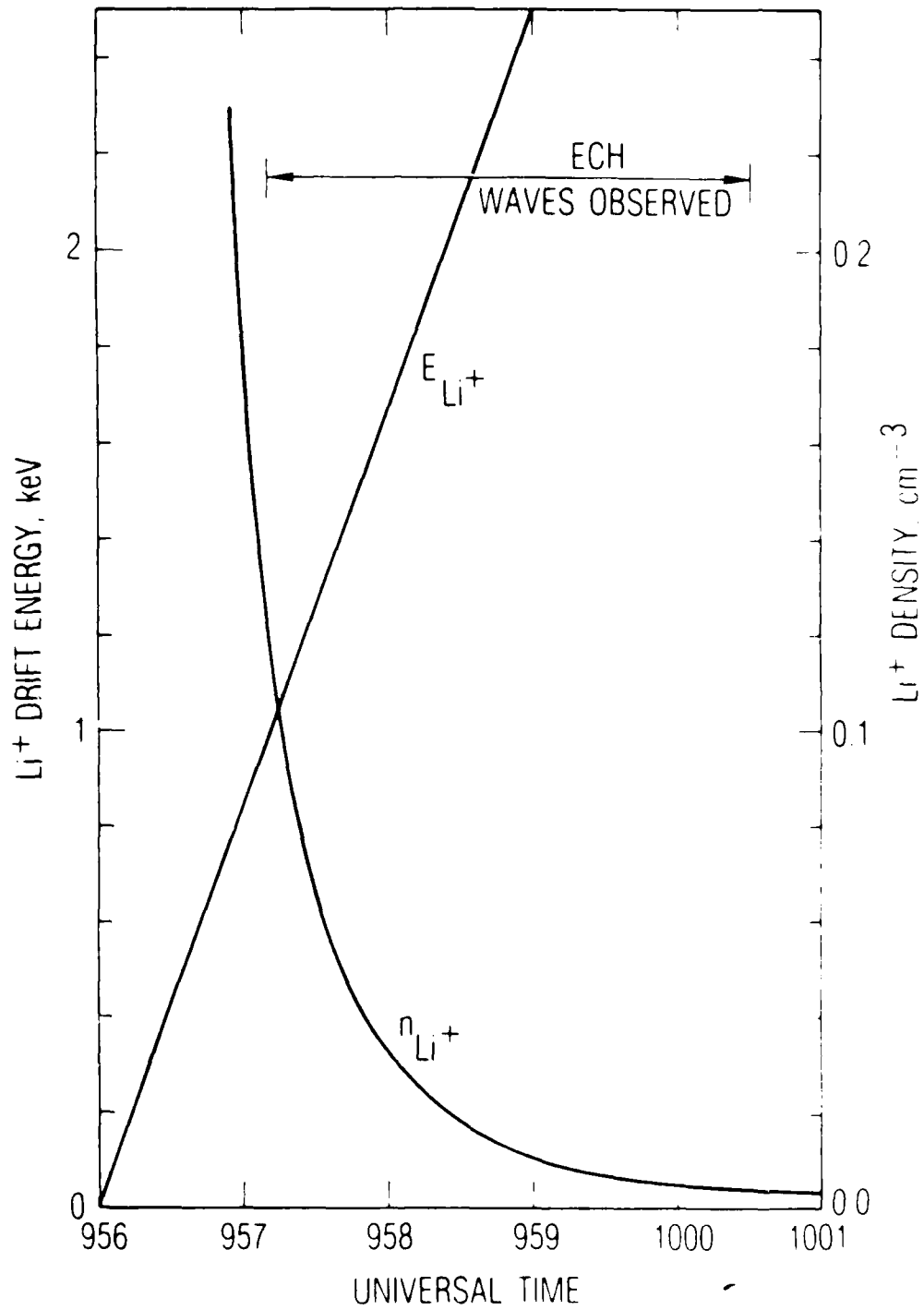


Figure 5. The Measured Number Density and Drift Energy of the Lithium Ions During the ECH Emissions

as a function of time the observed drift energy and density of the ions. The drift energies of the ions correspond to drift velocities in the range 166-332 km/s. The time interval in which the ECH waves were detected is marked at the top of the figure. The energy of the ions increases linearly with time, implying a linear increase in the distance over which they have been accelerated by the field. This result is consistent with a constant cloud expansion velocity [Haerendel et al., 1985]. The rapidly decreasing density reflects the expanding neutral lithium cloud producing fewer and fewer ions. At later times lithium ions of much higher energy were detected by the IRM [Mobius et al., 1985]. The temperature of the lithium beam was below the resolution of the IRM instruments. It can therefore be assumed that this temperature is between the photoionization energy of the lithium and the lower energy threshold of the instruments (0.2-2 eV).

Table 1 summarizes the particle observations during the ECH emissions. The electron distribution is assumed to be composed of a warm component plus a smaller cold component, both streaming at the solar wind velocity. This drift is approximately 187 km/s parallel and 420 km/s perpendicular to the magnetic field. The warm electron component is isotropic with a temperature of 18 eV and a density of 6 cm^{-3} . The cold component is assumed to be of temperature 1 eV and density in the range $0-2 \text{ cm}^{-3}$ to bring the total electron density up to 8 cm^{-3} . The characteristics of the solar wind proton distribution are also shown in Table 1. The lithium ion distribution is an isotropic beam whose density and drift perpendicular to the magnetic field follow the curves shown in Figure 5. The temperature of the lithium may be assumed to be in the range 0.2-2.0 eV.

Table 1.

Plasma Parameters During the ECH Emissions.

Solar Wind	
Total Velocity	460 km/s
Perpendicular Velocity	420 km/s
Parallel Velocity	187 km/s
Total Electron Density	8.2 cm ⁻³
Cool Electron Density	8 cm ⁻³
Cool Electron Temperature	18 eV
Warm Electron Density	0.2 cm ⁻³
Warm Electron Temperature	26 eV
Li ⁺ Density	0.03-0.1 cm ⁻³
Li ⁺ Temperature	0.2-1 eV
Li ⁺ Drift Velocity	166-332 km/s

MODEL RESULTS

There are several plasma microinstabilities which could produce electrostatic wave emissions with an electron cyclotron harmonic structure in the frequency spectrum. The most well known are a class of instabilities that use the free energy of a positive velocity gradient in the electron distribution function perpendicular to the ambient magnetic field. An example of this type is the loss-cone instability, which is often cited as the source of $n+1/2$ harmonics in the magnetosphere (for a complete review see Kennel and Ashour-Abdalla, 1984). In this case, however, the plasma observations show no evidence of any perpendicular anisotropy in the electron distribution.

A better candidate for the source of the waves is the electron cyclotron drift instability. This process uses the free energy of a relative ion-electron drift perpendicular to the magnetic field to amplify electron cyclotron mode waves. If $T_e \sim T_i$ the wave growth is due to ion Landau damping of the negative energy electron cyclotron mode. This instability has been proposed to generate the electrostatic turbulence observed near the earth's bow shock [Wu et al., 1984]. Recent theoretical investigations have shown, however, that this process may be stabilized by the field and plasma gradients of the shock wave [Zhou et al., 1984]. If $T_e \gg T_i$ the instability is caused by the resonant coupling of the negative energy electron cyclotron mode and the Doppler-shifted ion acoustic mode [Lampe et al., 1972]. This is the case which is applicable to the AMPTE release since the lithium ions are deposited in the solar wind with a temperature that is very low compared to the solar wind electrons. The stability of the system depends

primarily on the magnitude of the relative perpendicular velocity of the ions and electrons.

Figure 6 shows the vector geometry involved in the calculation of this parameter in the frame of reference of the IRM. The rectangular coordinate system has been rotated so that the interplanetary magnetic field \vec{B} is aligned with the y-axis and the solar wind velocity vector \vec{V}_{sw} lies in the z-y plane. The angle between the interplanetary magnetic field and the solar wind velocity is denoted by $\theta \sim 66^\circ$. The components of the velocity parallel and perpendicular to \vec{B} are shown in the figure as \vec{V}_{sw} and \vec{V}_{sw} . The solar wind convection electric field is $\vec{E}_{sw} = -\vec{V}_{sw} \times \vec{B}$, and it is directed along the x-axis. This electric field accelerates the lithium ions resulting in the lithium ion drift velocity \vec{V}_1 . The difference in velocity between these ions and the solar wind electrons in the electron frame is $\vec{V}_{1e} = \vec{V}_1 - \vec{V}_{sw}$. This vector is shown in the figure as perpendicular and parallel components. The perpendicular component is aligned in the x-z plane. The drift velocities corresponding to the energies of the ions shown in Figure 4 are 166 - 332 km/s. The wave vector of largest growth rate due to the electron cyclotron drift velocity is parallel to \vec{V}_{1e} . A cone of wave vectors around \vec{V}_{1e} , as shown in the figure, will have positive growth rates. The angular width of this cone is determined by electron cyclotron damping [Wong, 1970].

A model calculation has been performed to compare the linear growth rate and frequency of this instability to the observed ECH emissions. The velocity distributions of the solar wind electrons and the lithium ions were modeled as isotropic drifting Maxwellian

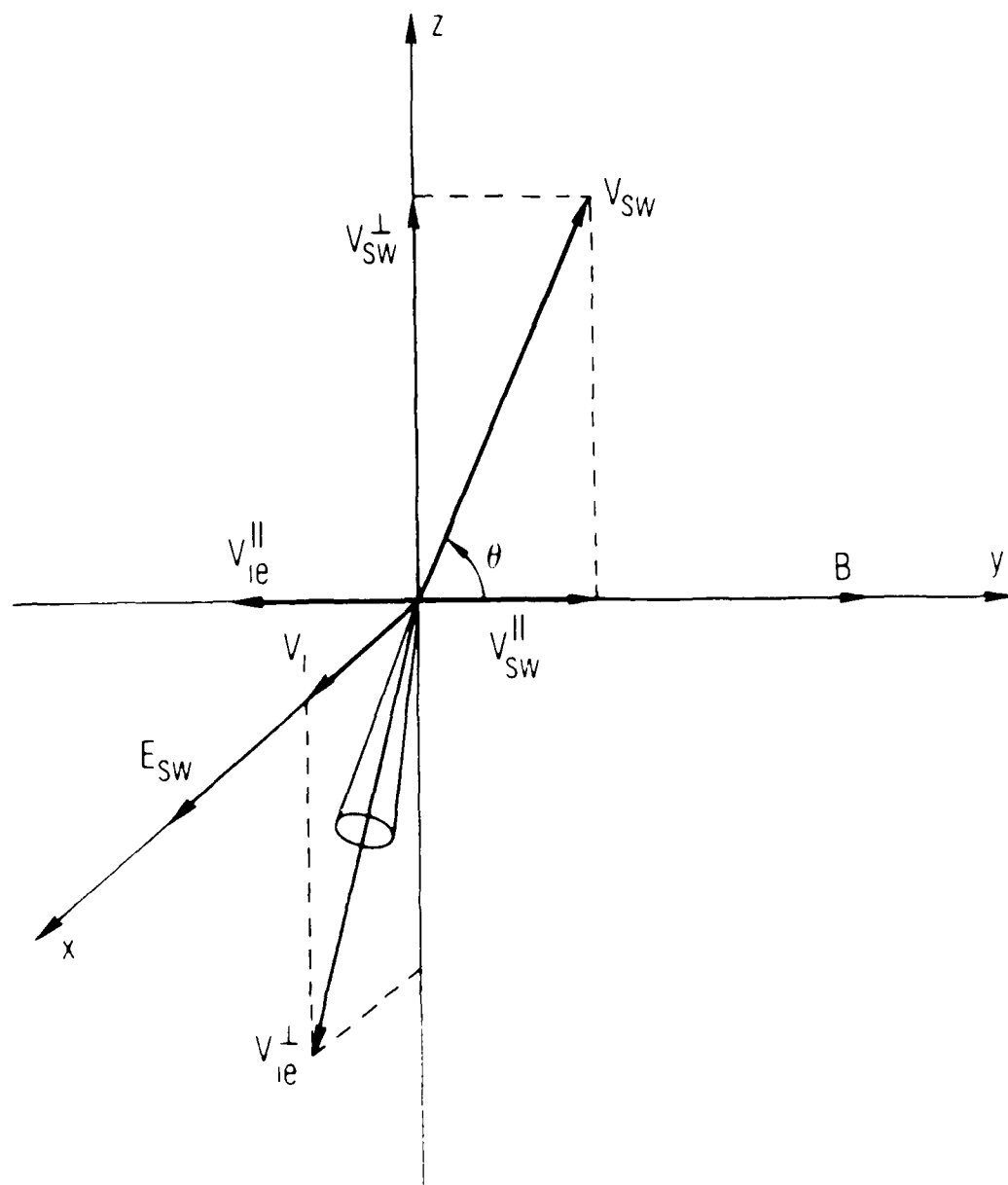


Figure 6. Schematic Diagram of the Vector Geometry Needed to Compute the Relative Velocity of the Lithium Ions and the Solar Wind Electrons

distributions. At frequencies above the electron cyclotron frequency the solar wind protons provide only a neutralizing background, so this species was neglected in the calculation. The densities and temperatures of the model were adjusted to agree with the observations. The ranges of parameters used are listed in Table 1. The lithium ion distribution was assumed to be unmagnetized so that it took the form of a perpendicular beam. This assumption requires that the growth rate of the instability be much larger than the ion cyclotron frequency. The electrostatic dispersion relation was solved numerically as a function of the parallel and perpendicular wave vector components.

Figure 7 shows the calculated frequency and the relative growth rate for the first four harmonic bands as a function of the almost perpendicular wave vector. The plasma parameters used in the calculation correspond to those present at the start of the observed waves and a lithium beam temperature of 2 eV. The harmonics of the cyclotron frequency are drawn as dashed lines. The diagonal line across the upper panel represents the frequency in resonance with the lithium ion beam. Just above each point where this line intersects the real frequency there is a region of positive growth due to the ions. The temporal growth rates are plotted in the bottom panel. The maximum growth rates of the waves approach one percent of the real frequency, which is more than enough to account for the amplitude of the observed waves. The small extent of the positive growth region in wave vector space is a result of the extremely low lithium temperature. The frequency dispersion of the waves appears very similar to the ordinary electron cyclotron harmonics because the ion density is too small to affect the real part of the dispersion relation.

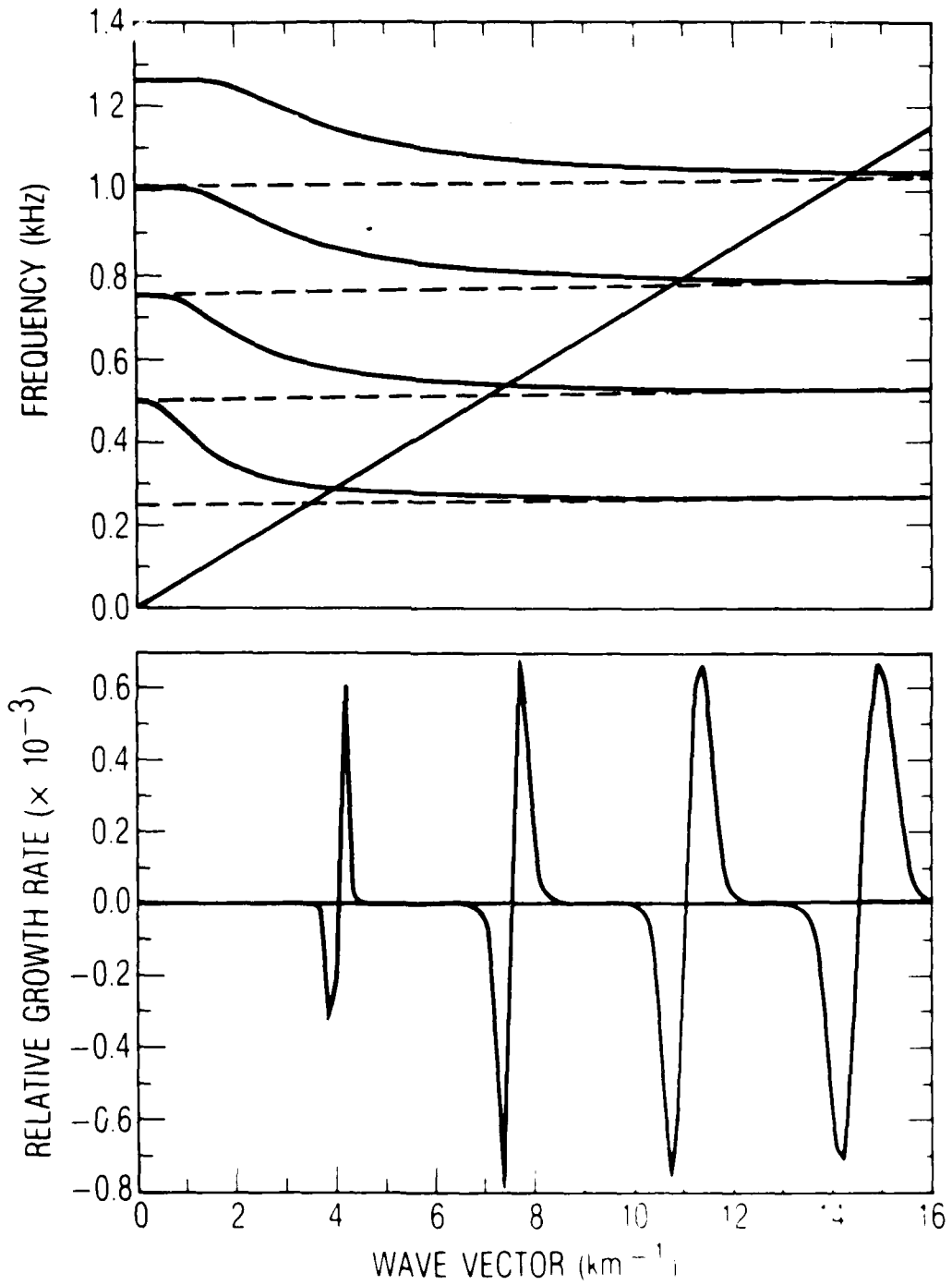


Figure 7. Model Frequencies and Temporal Growth Rates for the First Four Harmonics Due To the Electron Cyclotron Drift Instability

The number of unstable harmonics is set by a Debye length criterion on the wave vector. The wave vector of the unstable waves must be less than the reciprocal of the Debye length. In this case the Debye length of the plasma is very small ($\lambda_D \sim 0.01$ km), so that the number of unstable harmonics is extremely large ($n \sim 25$). The observation of only six emission bands may indicate that some additional damping mechanism is operative at the higher harmonics.

This calculation was performed in the frame of reference of the electrons. In the frame of the spacecraft the frequencies of the waves will be Doppler shifted downward by the perpendicular velocity of the solar wind \vec{V}_{sw} . This frequency shift is a major fraction of the computed frequency so that all the emissions should be observed below the electron cyclotron frequency. For example, in the case shown above, the calculated frequency in the spacecraft frame is approximately 13% of the frequency in the electron frame. The resulting spectrum consists of a set of evenly spaced lines with the fundamental emission at 34 Hz. The observation of the emissions above the cyclotron frequency is inconsistent with this calculation.

This inconsistency between the observed wave spectrum and the calculated unstable spectrum may be resolved by several possibilities. The instability investigated above could generate waves with wave vectors perpendicular to the solar wind velocity. The Doppler shift of waves in that direction would be very small. However, this would imply that waves in a wide range of directions are equally unstable, and the Doppler shift would produce a spectrally broadened emission instead of narrow bands. An alternative explanation requires the existence of a

population of electrons which is stationary in the spacecraft frame. This electron population would resonate with the ion beam and generate the cyclotron waves the same manner as the solar wind electrons. The lithium photoionization reaction could provide a source for such an electron component. In the above calculation it was assumed that these electrons were swept up by the solar wind immediately. But the ionization reaction is proceeding continuously throughout the observation interval. This would produce a long tenuous tail aligned with the solar wind velocity. The exact effect of this population on the stability of the system may be difficult to estimate due to the cycloidal motion of these electrons and also heating processes that may be operative. The third possibility for the generation of the ECH waves is an unobserved perpendicular velocity gradient in the electron distribution. The photoionization population mentioned above may provide enough positive gradient to destabilize the plasma in a manner similar to the loss cone process.

CONCLUSION

Electrostatic electron cyclotron wave emissions are observed in connection with the second lithium release by the AMPTE-IRM spacecraft into the solar wind. A linear analysis of the plasma system during the emissions indicates that large wave growth rates were present due to the electron cyclotron drift instability. However, the observed lack of a major downward Doppler shift is inconsistent with the theory. The several explanations of this problem discussed involve velocity space anisotropies due to the electrons released by the lithium photoionization reaction.

REFERENCES

- Anderson, R. R., D. A. Gurnett, B. Haeusler, H. C. Koons, R. Holzworth, R. Treumann, O. H. Bauer, G. Haerendel, H. Luhr, L. J. Woolliscroft, M. P. Gough, Electron number density from the AMPTE-IRM plasma wave experiment during solar wind lithium releases, J. Geophys. Res. (submitted for publication), 1985.
- Bryant, D. A., S. M. Krimigis, and G. Haerendel, Outline of the active magnetospheric particle tracer explorers (AMPTE) mission, IEEE Trans. Geosci. Remote Sensing, GE-23, 177, 1985.
- Gurnett, D. A., T. Z. Ma, R. R. Anderson, O. H. Bauer, G. Haerendel, B. Haeusler, G. Paschmann, R. Treumann, H. Koons, R. Holzworth, and H. Luhr, Analysis and interpretation of the shock-like electrostatic noise associated with the AMPTE solar wind lithium releases, J. Geophys. Res. (submitted for publication), 1985.
- Haerendel, G., Interaction of lithium plasma clouds with the interplanetary medium, J. Geophys. Res. (submitted for publication), 1985.
- Haerendel, G., A. Valenzuela, H. Foppl, B. Haeusler, F. Melzner, G. Paschmann, and J. Stocker, Physical properties of the lithium injection experiments in the solar wind, J. Geophys. Res. (submitted for publication), 1985.

Hall, D. S., D. A. Bryant, C. P. Chaloner, D. R. Lepine, and R. Bingham, AMPTE-UKS electron measurements during the lithium releases of 11 and 20 september 1984, J. Geophys. Res. (submitted for publication), 1985.

Haeusler B., L. J. Woolliscroft, R. R. Anderson, D. A. Gurnett, R. H. Holzworth, H. C. Koons, O. H. Bauer, G. Haerendel, R. A. Treumann, P. J. Christiansen, A. G. Darbyshire, M. P. Gough, S. R. Jones, A. J. Norris, H. Luhr, and N. Klocker, Plasma waves observed by the IRM and UKS spacecraft during the AMPTE solar wind lithium releases: overview, J. Geophys. Res. (submitted for publication), 1985.

Kennel, C. F., and M. Ashour-Abdalla, Electrostatic waves and the strong diffusion of magnetospheric electrons, in Magnetospheric Plasma Physics, edited by A. Nishida, p. 245, D. Reidel, Dordrecht, Holland, 1982.

Krimigis, S. M., G. Haerendel, R. W. McEntire, G. Paschmann, D. A. Bryant, The Active Particle Tracer Explorers (AMPTE) Program, EOS, 63, 843, 1982.

Lampe, M., W. M. Manheimer, J. B. McBride, J. H. Orens, K. Papadopoulos, R. Shanny, and R. N. Sudan, Theory and simulation of the beam cyclotron instability, Phys. Fluids, 15, 662, 1972.

H. Luhr, D. J. Southwood, N. Klocker, M. Acuna, B. Haeusler, W. A. C. Mier-Jedrzejowicz, R. P. Rijnbeek, and M. Six, In-situ magnetic field measurements during AMPTE solar wind Li^+ - releases, J. Geophys. Res. (submitted for publication), 1985.

- Mobius, E., D. Hovestadt, B. Klecker, M. Scholer, G. Gloeckler, F. M. Ipavich, H. Luhr, Observation of lithium pick-up ions in the 5 to 20 keV energy range following the AMPTE solar wind releases, J. Geophys. Res. (submitted for publication), 1985.
- Wong, H. V., Electrostatic electron-ion streaming instability, Phys. Fluids, 13, 757, 1970.
- Wu, C. S., Y. M. Zhou, S. T. Tsai, P. Rodriguez, M. Tanaka, K. Papadopoulos, K. Akimoto, C. S. Lin, M. M. Leroy, and C. C. Goodrich, Microinstabilities associated with a high mach number, perpendicular shock, Space Sci. Rev., 37, 63, 1984.
- Zhou, Y. M., Y. Y. Li, and C. S. Wu, Stabilizing effects of a magnetic field gradient in a perpendicular shock wave on electron-cyclotron-drift instability, Phys. Fluids, 27, 2049, 1984.

LABORATORY OPERATIONS

The Aerospace Corporation functions as an "architect-engineer" for national security projects, specializing in advanced military space systems. Providing research support, the corporation's Laboratory Operations conducts experimental and theoretical investigations that focus on the application of scientific and technical advances to such systems. Vital to the success of these investigations is the technical staff's wide-ranging expertise and its ability to stay current with new developments. This expertise is enhanced by a research program aimed at dealing with the many problems associated with rapidly evolving space systems. Contributing their capabilities to the research effort are these individual laboratories:

Aerophysics Laboratory: Launch vehicle and reentry fluid mechanics, heat transfer and flight dynamics; chemical and electric propulsion, propellant chemistry, chemical dynamics, environmental chemistry, trace detection; spacecraft structural mechanics, contamination, thermal and structural control; high temperature thermomechanics, gas kinetics and radiation; cw and pulsed chemical and excimer laser development including chemical kinetics, spectroscopy, optical resonators, beam control, atmospheric propagation, laser effects and countermeasures.

Chemistry and Physics Laboratory: Atmospheric chemical reactions, atmospheric optics, light scattering, state-specific chemical reactions and radiative signatures of missile plumes, sensor out-of-field-of-view rejection, applied laser spectroscopy, laser chemistry, laser optoelectronics, solar cell physics, battery electrochemistry, space vacuum and radiation effects on materials, lubrication and surface phenomena, thermionic emission, photo-sensitive materials and detectors, atomic frequency standards, and environmental chemistry.

Computer Science Laboratory: Program verification, program translation, performance-sensitive system design, distributed architectures for spaceborne computers, fault-tolerant computer systems, artificial intelligence, microelectronics applications, communication protocols, and computer security.

Electronics Research Laboratory: Microelectronics, solid-state device physics, compound semiconductors, radiation hardening; electro-optics, quantum electronics, solid-state lasers, optical propagation and communications; microwave semiconductor devices, microwave/millimeter wave measurements, diagnostics and radiometry, microwave/millimeter wave thermionic devices; atomic time and frequency standards; antennas, rf systems, electromagnetic propagation phenomena, space communication systems.

Materials Sciences Laboratory: Development of new materials: metals, alloys, ceramics, polymers and their composites, and new forms of carbon; non-destructive evaluation, component failure analysis and reliability; fracture mechanics and stress corrosion; analysis and evaluation of materials at cryogenic and elevated temperatures as well as in space and enemy-induced environments.

Space Sciences Laboratory: Magnetospheric, auroral and cosmic ray physics, wave-particle interactions, magnetospheric plasma waves; atmospheric and ionospheric physics, density and composition of the upper atmosphere, remote sensing using atmospheric radiation; solar physics, infrared astronomy, infrared signature analysis; effects of solar activity, magnetic storms and nuclear explosions on the earth's atmosphere, ionosphere and magnetosphere; effects of electromagnetic and particulate radiations on space systems; space instrumentation.

END

2-87

DTIC